

1 **Loss of the centrosomal protein ALMS1 alters lipid**
2 **metabolism and the regulation of extracellular**
3 **matrix-related processes**

4 Brais Bea-Mascato^{1,2}, Eduardo Gómez-Castañeda⁴, Yara E. Sánchez-Corrales³, Sergi
5 Castellano^{3,5}, Diana Valverde^{*1,2}

6

7 ¹ CINBIO, Universidad de Vigo, 36310, Spain.

8 ² Grupo de Investigación en Enfermedades Raras y Medicina Pediátrica, Instituto de
9 Investigación Sanitaria Galicia Sur (IIS Galicia Sur), SERGAS-UVIGO, Vigo, Spain

10 ³ Genetics and Genomic Medicine Department, Great Ormond Street Institute of Child
11 Health, University College London, London, United Kingdom

12 ⁴ Molecular and Cellular Immunology Section, Great Ormond Street Institute of Child
13 Health, University College London, London, United Kingdom

14 ⁵ UCL Genomics, Zayed Centre for Research into Rare Disease in Children, University
15 College London, London, United Kingdom

16 *Correspondence: Diana Valverde. Email dianaval@uvigo.es

17 CINBIO Facultad de Biología, Universidad de Vigo, Campus As Lagoas-Marcosende s/n,
18 36310 Vigo, Spain

19 Tel +34 986 811 953

20 **ABSTRACT:**

21 **Background:** Alström syndrome (ALMS) is a rare autosomal recessive disease that is
22 associated with mutations in *ALMS1* gene. The main clinical manifestations of ALMS are
23 retinal dystrophy, obesity, type 2 diabetes mellitus, dilated cardiomyopathy and multi-
24 organ fibrosis, characteristic in kidneys and liver. Depletion of the protein encoded by
25 *ALMS1* has been associated with the alteration of different processes regulated *via* the
26 primary cilium, such as the NOTCH or TGF- β signalling pathways. However, the cellular
27 impact of these deregulated pathways in the absence of *ALMS1* remains unknown.

28 **Methods:** In this study, we integrated RNA-seq and proteomic analysis to determine the
29 gene expression profile of hTERT-BJ-5ta *ALMS1* knockout fibroblasts after TGF- β
30 stimulation. In addition, we studied alterations in cross-signalling between the TGF- β
31 pathway and the AKT pathway in this cell line.

32 **Results:** We found that *ALMS1* depletion affects the TGF- β pathway and its cross-
33 signalling with other pathways such as PI3K/AKT, EGFR1 or p53. In addition, alterations
34 associated with *ALMS1* depletion clustered around the processes of extracellular matrix
35 regulation and lipid metabolism in both the transcriptome and proteome. By studying
36 the enriched pathways of common genes differentially expressed in the transcriptome
37 and proteome, collagen fibril organisation, β -oxidation of fatty acids and eicosanoid
38 metabolism emerged as key processes altered by the absence of *ALMS1*. Finally, an
39 overactivation of the AKT pathway was determined in the absence of *ALMS1* that could
40 be explained by a decrease in *PTEN* gene expression.

41 **Conclusion:** *ALMS1* deficiency disrupts cross-signalling between the TGF- β pathway and
42 other dependent pathways in hTERT-BJ-5ta cells. Furthermore, altered cross-signalling
43 impacts the regulation of extracellular matrix-related processes and fatty acid
44 metabolism, and leads to over-activation of the AKT pathway.

45 **Keywords:** *ALMS1*, TGF- β , AKT, primary cilia, ciliopathy, ECM, lipid metabolism, Alström
46 syndrome.

47 INTRODUCTION:

48 Alström syndrome (ALMS, OMIM #203800) is a rare disease caused by mutations in the
49 *ALMS1* gene. The subcellular localisation of the ALMS1 protein in the basal body of the
50 primary cilium, composed of two centrioles, classified ALMS as a ciliopathy (Hearn et al.,
51 2005; Knorz et al., 2010; Jagger et al., 2011; Kobayashi and Dynlacht, 2011). Ciliopathies
52 are a group of diseases on which, the normal function and assembly of the primary cilia
53 is affected. This ciliopathy is clinically characterised by the development of retinal
54 dystrophy, type 2 diabetes mellitus (T2DM), obesity, dilated cardiomyopathy (DCM),
55 hearing loss and multi-organ fibrosis affecting kidneys, liver and lungs (Collin et al., 2002;
56 Zulato et al., 2011; Hearn, 2018).

57 Primary cilia are sensory organelles formed by microtubules protruding from the cell
58 membrane. They are essential for a variety of physiological and developmental
59 processes such as the control of cell cycle, migration and differentiation (Christensen et
60 al., 2017; Pala et al., 2017; Anvarian et al., 2019). They also play a role in the regulation
61 of various signalling pathways, such as WNT, Sonic Hedgehog (SHh), transforming
62 growth factor β (TGF- β) and other G-protein-coupled receptor-regulated pathways
63 (Ishikawa and Marshall, 2011; May-Simera et al., 2017, 2018; Pala et al., 2017; Anvarian
64 et al., 2019).

65 The role of the ALMS1 protein is still unclear, with some (Graser et al., 2007; Li et al.,
66 2007; Knorz et al., 2010) but not all (Collin et al., 2005, 2012; Hearn et al., 2005; Chen et
67 al., 2017) studies suggesting a role in ciliogenesis. ALMS1 depletion, however, affects
68 several signalling pathways regulated through primary cilia, such as the NOTCH and TGF-
69 β pathways (Leitch et al., 2014; Álvarez-Satta et al., 2021; Bea-Mascato et al., 2022). In
70 the NOTCH signalling pathway, ALMS1 depletion leads to the accumulation of receptors
71 in late endosomes. However, it does not affect the recycling of these receptors in the
72 cell line hTERT-RPE1 (Leitch et al., 2014). In the TGF- β pathway, inhibition of *ALMS1*
73 expression lowers phosphorylation/activation of SMAD2 in hTERT-RPE1 (Álvarez-Satta
74 et al., 2021), which could inhibit the canonical TGF- β pathway. Similar results have been
75 described when abolishing other centrosomal proteins. For example, depletion of
76 CEP128 decreases SMAD2 phosphorylation in zebrafish, hTERT-RPE1 and ciliated human

77 foreskin fibroblasts (hFF) after TGF- β activation (Mönnich et al., 2018). However, these
78 alterations were not observed in ALMS1 knockout models in HeLa or hTERT-BJ-5ta (Bea-
79 Mascato et al., 2022). In these models the only alteration detected in the canonical
80 pathway was a slight decrease in SMAD3 phosphorylation/activation in the hTERT-BJ-
81 5ta model (Bea-Mascato et al., 2022). This suggests that alterations in the TGF- β
82 pathway in the absence of ALMS1 may have a greater impact on other signalling
83 pathways that cross-signal with this pathway such as PI3K/AKT or MAPKs (p38, c-JNKs
84 and others) (Finsson et al., 2020).

85 Despite advances in recent years, little is known about the role of ALMS1 in primary cilia
86 and its regulated signalling pathways. Here, we investigate at the RNA and protein level
87 how the absence of ALMS1 expression in hTERT-BJ-5ta affects the TGF- β pathway and
88 other cellular processes.

89 **MATERIALS AND METHODS:**

90 **Cell culture:**

91 hTERT-BJ-5ta human dermal fibroblasts and HeLa cell lines from American Type Culture
92 Collection (ATCC) were used for this study. A 4:1 composite medium of Dulbecco's
93 minimum essential medium (DMEM, Gibco, Invitrogen, NY, USA) and Medium 199,
94 Earle's Salts (Gibco, Invitrogen, NY, USA), supplemented with 10% fetal bovine serum
95 (FBS) (Gibco, Invitrogen, NY, USA) and 2% penicillin/streptomycin (P/S) (Gibco,
96 Invitrogen, NY, USA) was used to maintain hTERT-BJ-5ta. DMEM medium supplemented
97 with 10% FBS and 2% P/S was used for the HeLa cells. Both cell lines were cultured at
98 37°C with 5% CO₂.

99 **RNA extraction:**

100 Initially, 3x10⁵ BJ-5ta cells were seeded in 6-well plates by triplicate in DMEM:199
101 10%FBS 2% P/S. After 24h a change of medium was made by adding DMEM:199 2% P/S
102 without FBS and cells were incubated overnight for serum starvation. Next day, TGF- β
103 pathway was stimulated by adding rhTGF- β 1 ligand (2ng/mL; R&D Systems; 240-B) for
104 24 hours. Then, the medium was removed, and wells were washed twice with PBS. Cells

105 were harvested in a tube of 1.5 mL after scraping them on PBS. The NYZ total RNA
106 isolation kit (NYZtech, Lisboa, Portugal) was applied following the manufacturing
107 protocol for RNA extraction. Finally, RNA was eluted, and sample concentrations were
108 measured with nanodrop (Thermo Fisher, Waltham, USA).

109 **RNA-seq and library construction:**

110 RNA quality control was performed using Bioanalyzer (Agilent, Santa Clara, USA), finding
111 a RIN \geq 7. Then, RNA enrichment was carried out with the Dynabeads mRNA direct Micro
112 kit (Life Technologies, Carlsbad, USA) following manufacturer's protocol. Sequencing
113 libraries were constructed from cDNA using the Ion Total RNA-seq Kit v2 with ERCC RNA
114 Spike-in Control mix (Thermo Fisher, Waltham, USA). 25 μ L of each library was
115 sequenced using a PI V2 chip in an Ion Proton Sequencer (Thermo Fisher, Waltham,
116 USA).

117 After sequencing, fastq files were analysed in the Finisterrae II computer cluster of the
118 "Centro de Supercomputación de Galicia" (CESGA). FastQC ([http://www](http://www.bioinformatics.babraham.ac.uk/projects/fastqc)
119 [.bioinformatics.babraham.ac.uk/projects/fastqc](http://www.bioinformatics.babraham.ac.uk/projects/fastqc)) and MultiQC (Ewels et al., 2016) were
120 used to determine the quality of the samples (**Figure S1 A**). High-quality reads were
121 aligned with STAR software (Dobin et al., 2013) using the primary assembly of Homo
122 sapiens genome GRCh38.p13 (Gencode v32). We generated a count matrix using the
123 HTSeq software (Anders et al., 2015). Downstream analysis was performed with the
124 following R (version 4.0.5) packages: DESeq2 (Love et al., 2014) to detect differentially
125 expressed genes (DEG; **Figure S1 B-D; Table S1**); and EnrichR (Kuleshov et al., 2016) for
126 enrichment analysis of GO terms and Pathways, collected from different databases
127 (Bioplanet, KEGG, MSigDB and wikipathway) (**Table S3**). P-values were calculated using
128 Fisher's exact test and corrected using Benjamini-Hochberg (FDR). Finally, ggplot and
129 pheatmap were used for the visualisation of the results (Wickham, 2016). To validate
130 our homemade DESeq2 pipeline, SARTools (Varet et al., 2016) was applied and the same
131 number of DEG was obtained.

132 The sequences generated in this work have been deposited in NCBI's Gene Expression
133 Omnibus (Barrett et al., 2013) and are accessible through GEO Series accession number
134 GSE209844.

135 **Protein extraction:**

136 BJ-5ta cells were seeded at 3×10^5 in 6-well plates by triplicate in DMEM:199 10%FBS
137 2%P/S. After 24 hours, FBS was removed from the medium and the cells were incubated
138 overnight for serum starvation. The next day, cells were stimulated with rhTGF- β
139 (2ng/mL) for 24 hours. After that, DMEM:199 was removed, and wells were washed
140 twice with PBS. Cells were scrapped in PBS. Then, they were pellet at 10000 rpm for 5
141 min in a Sigma® 1–14 K at 4°C and 100 μ L of RIPA buffer was added to each sample for
142 cell lysis. Samples were incubated on ice for 10 min in constant agitation. Finally, cell
143 debris was pelleted by centrifugation for 30 min at 12000 rpm and 4 °C. Samples were
144 aliquoted and stored at -80 °C until the next step of the protocol. Protein quantification
145 was performed by Bradford microplate assay using Bio-Rad protein assay (Bio-rad,
146 Hercules, USA).

147 **Label-free proteomic profiling:**

148 Label-free proteomic profiling was performed following the same protocol described in
149 (Bea-Mascato et al., 2022) with the corresponding quality controls (**Figure S2; Table S2**).
150 Ggplot and pheatmap were used for the results visualisation. Enrichment analysis was
151 performed using the same protocol as described for the transcriptome (**Table S4**). The
152 mass spectrometry proteomics data of this study have been deposited to the
153 ProteomeXchange Consortium via the PRIDE (Perez-Riverol et al., 2019) partner
154 repository with the dataset identifier PXD035708.

155 **Networks generation:**

156 For the generation of the different networks, we used the programme Cytoscape (3.9.0)
157 with Java (11.0.6). For the generation of the enriched route networks, the pipeline
158 described by Reimand et al.(Reimand et al., 2019) was used. Similarity coefficients
159 between nodes (minimum threshold of 0.375) were calculated using the arithmetic
160 mean between the overlap coefficient and the Jaccard index of the different significantly
161 enriched gene sets in the enrichment analysis (FDR < 0.05). After this procedure, the
162 clusters were annotated using the plugins ClusterMaker2, wordCloud and
163 autoanotation. The MCL algorithm was used via the ClusterMaker2 plugin to determine

164 the clusters and then wordCloud and autoannotation were used to annotate the
165 clusters. The settings were maintained to generate the networks of the different
166 datasets.

167 **p-AKT/AKT activation assays:**

168 Initially, about 3×10^6 BJ-5ta control and ALMS1 knockout (KO) cells were plated in
169 100mm dishes (Corning, NY, USA) in DMEM:199 2P/S% without FBS for serum
170 starvation. After 24h of incubation, the rhTGF- β 1 ligand was added at a final
171 concentration of 2ng/mL for 0-, 10-, 30-, and 90-min. Dishes were then washed 3 times
172 with PBS and harvested in 1mL of PBS, using a scraper. After that, cells were pelleted by
173 centrifugation in a Sigma® 1–14 K at 4°C, 7,400 \times g for 10 min and lysed on ice for 10 min
174 using 200 μ L of RIPA buffer, containing 1 mM sodium orthovanadate as phosphatase
175 inhibitor (Sigma-Aldrich, Missouri, USA) and 0.1% (v/v) protease inhibitor cocktail
176 (Merck, Darmstadt, Germany). To remove the pellet with cell debris not lysed with RIPA
177 buffer, samples were centrifuged at 4°C, 14,500 \times g for 30 min, and the supernatant was
178 collected in 1.5mL low binding tubes (Thermo Fisher, Waltham, USA). For protein
179 quantification, the Bio-Rad protein assay reagent was used in a microplate assay. Finally,
180 samples were stored at -80°C until analysis.

181 **SDS-PAGE, Western blot and quantification:**

182 Samples were prepared mixing 20 μ g of protein from each sample with 6.25 μ L of
183 Laemmli Buffer 4X (Biorad, Hercules, USA), 1.25 μ L β -mercaptoethanol (BME) and H₂O_d
184 up to a final volume of 25 μ L. After that, samples were boiled at 97°C for 5 min and run
185 on a 12% Mini-PROTEAN® TGX™ Precast Gel (Biorad, Hercules, USA) for 1 hour at 150V.
186 Proteins were then transferred to a 0.2 μ m polyvinylidene fluoride (PVDF) membrane
187 using the Trans-Blot® Turbo™ Transfer System (Biorad, Hercules, USA) following the
188 mixed molecular weight (MW) protocol. Membranes were blocked with in-house TBS-T
189 buffer [TBS/0.1% (v/v) Tween-20] with 5% (w/v) milk for 90min at room temperature
190 (RT). Incubation with the primary antibody was carried out in blocking solution (TBS-T
191 5% milk) overnight at 4°C. For this assay, the following antibodies were used: anti-AKT
192 (1:5000, Abcam, 179463) and anti-p-AKT (1:5000, Abcam, 222489).

193 The next day, the membranes were washed 3 times with PBS. They were then incubated
194 with the secondary antibody in a blocking solution for 1 hour at RT. Goat anti-rabbit IgG
195 H&L (HRP) (Abcam, 205718) was used as a secondary antibody in this assay at 1:5000
196 for p-AKT and 1:10000 for AKT.

197 Finally, Clarity western ECL substrate (Biorad, Hercules, USA) was used to develop the
198 membranes. The photos were taken by exposure on the ChemiDoc system (Biorad,
199 Hercules, USA) after 5 minutes of incubation with the substrate. Quantification of bands
200 was carried on Image Lab software (Biorad, Hercules, USA) using the method of total
201 protein.

202 **Fluorescent preparations:**

203 2×10^4 HeLa cells (WT and *ALMS1* KO) were seeded in μ -Slide 8-well chambers (IBIDI,
204 Germany). After 24 hours cells were transfected with pcDNA3 GFP-PTEN using
205 Lipofectamine 3000 (Thermo Fisher, Waltham, USA) following the manufacturer's
206 protocol. Cells were incubated overnight at 37°C with 5% CO₂. The following day, the
207 medium was changed by adding DMEM 2% P/S and 2%FBS. In addition, rhTGF- β was
208 added to the corresponding wells at a final concentration of 2ng/mL and the plates were
209 incubated again overnight under the same conditions. Finally, on the fourth day, the
210 preparations were marked, fixed and mounted, following the protocol detailed below.

211 200 μ L of DMEM medium per well containing CellMask (Thermo Fisher, Waltham, USA)
212 at a 1:1000 dilution were added and incubated for 10min at 37°C in the dark. After two
213 washes with PBS, the cells were fixed with 150 μ L of 4% paraformaldehyde (PFA) in a
214 1:10 dilution of DMEM medium and incubated for 10min. The PFA diluted in DMEM was
215 removed with 2 washes with PBS and 200 μ L of PBS with DAPI was added at a final
216 concentration of 1 μ g/mL, followed by a 20min incubation in the dark. Finally, the wells
217 were washed 3 times with PBS to remove the DAPI solution and the samples were
218 mounted with 3 drops of Prolong. After incubation for 1 hour at 4°C, the samples were
219 analysed on the Nikon NIE microscope. (Nikon, Tokyo, Japan).

220 This experiment was performed in duplicate on 2 alternate days adding 2 wells in each
221 experiment for each treatment and cell line (WT and KO).

222 GFP-PTEN was a gift from Alonzo Ross (Addgene plasmid # 13039;
223 <http://n2t.net/addgene:13039>; RRID: Addgene_13039)

224 **Image acquisition, processing and analysis:**

225 The images were taken with the Nikon NIE direct microscope at 20X, using the RGB
226 channels for the acquisition of DAPI (Blue), GFP-PTEN with FITC (Green) and CellMask
227 with TRITC (Red). After that, all the images were processed with Fiji (Java 8 version)
228 (Schindelin et al., 2012). The background was subtracted from all images, the resolution
229 was set to 4908x3264 (0.25microns/pixel) and the RGB channels were grouped with the
230 "Merge Channels" option to create the compositions, maintaining the independence of
231 the channels. Cell segmentation was then performed using the biodock platform
232 (<https://www.biodock.ai/>). Cells were filtered by size to remove any debris that could
233 have been detected as cells by the algorithm. Finally, the signal from the 550 cells with
234 the highest GFP intensity was normalised against the mean of TGF- β stimulated control
235 to obtain the normalised fluorescence values.

236 **Statistical analysis:**

237 The proteomic study involved several statistical analyses and data transformations. The
238 data were first normalized using a variance stabilisation procedure (VSN). Data
239 imputation for missing values was carried out using the Minprob approach with a q-
240 value of less than 0.01. Finally, differential expression analysis was performed using the
241 linear protein models of the limma package (Ritchie et al., 2015) included in the DEP R
242 package (Zhang et al., 2018).

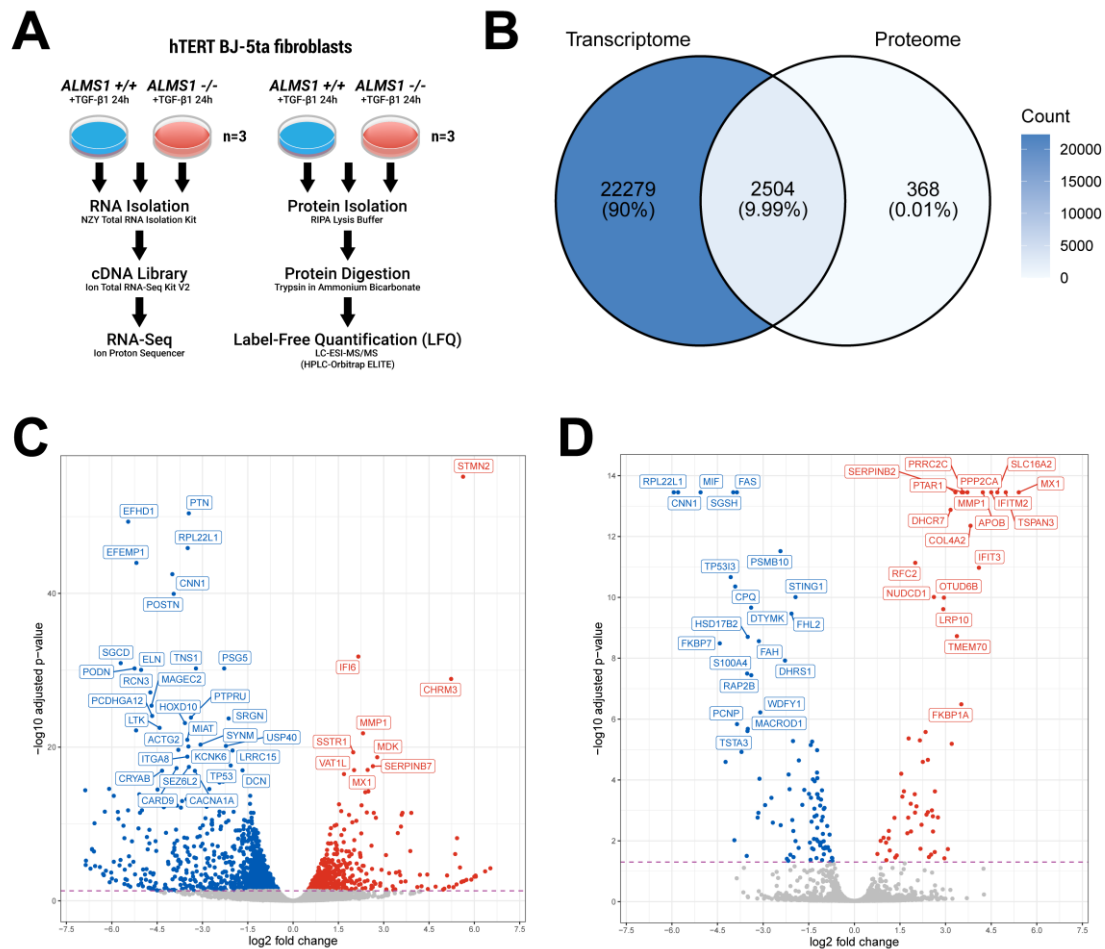
243 Transcriptomic normalisation and analysis were performed using DESeq2 (Love et al.,
244 2014). An FDR value < 0.05 was used to determine differentially expressed genes.

245 To analyse statistical differences in the Western blot data, a t-student with a Benjamini,
246 Krieger, & Yekutieli two-stage correlation was used. Finally, the fluorescence imaging
247 results were analysed with a 2-way ANOVA.

248

249 RESULTS:

250 Inhibition of *ALMS1* gene expression causes several alterations 251 of the transcriptome and proteome:



252

253 **Figure 1.** Differential expression analysis in the BJ-5ta *ALMS1* knockout cell line by RNA-seq and
254 LFQ-proteomics. **(A)** Illustration of the experimental design and procedure followed in this study.
255 **(B)** Total overlap between genes identified in the transcriptome and the proteome. **(C)** Volcano-
256 plot of differentially expressed genes (FDR < 0.05) in RNA-seq, highlighting the 40 most
257 significant genes. **(D)** Volcano-plot of differentially expressed proteins (FDR < 0.05) in the
258 proteome, highlighting the 40 most significant protein-coding genes.

259 In this study, we generated a multi-omics dataset (total RNA-seq and LFQ-proteomic
260 analysis) on an hTERT fibroblast cell line (WT/CT and *ALMS1* KO). This cell line was

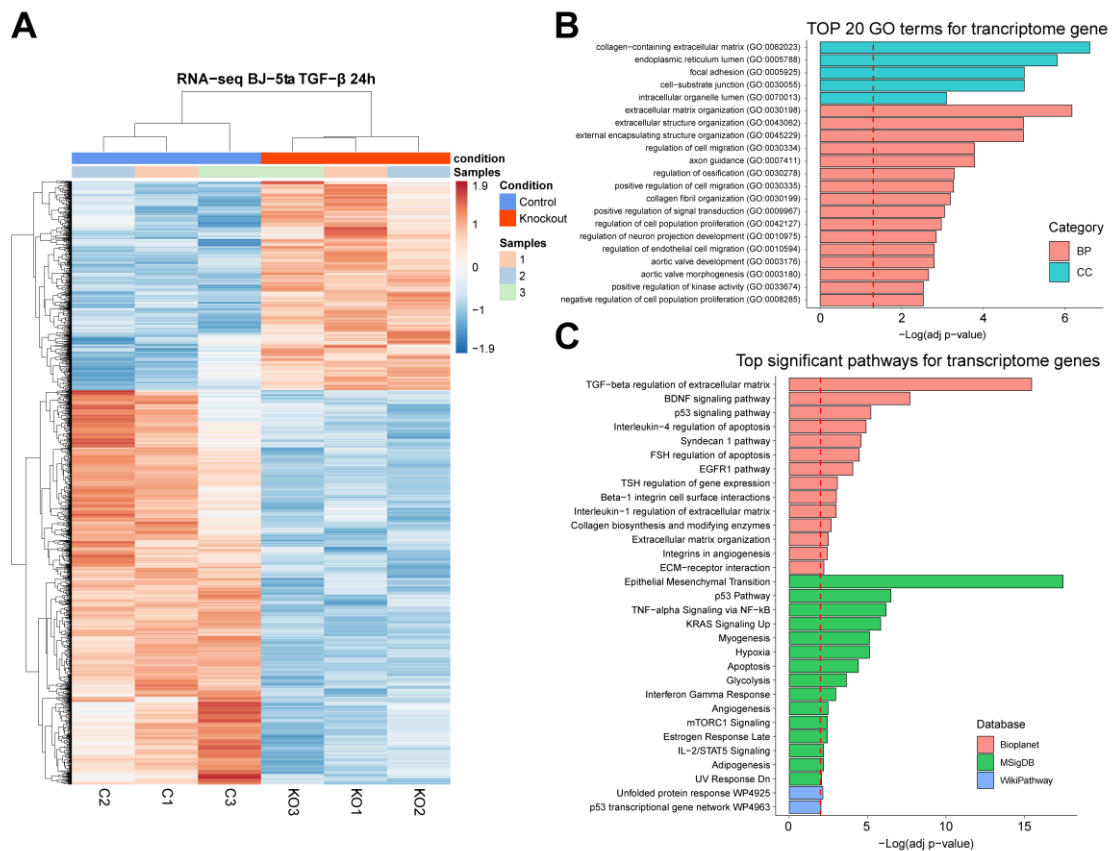
261 previously stimulated with TGF- β 1 ligand to identify alterations related with TGF- β
262 pathway (**Figure 1A**).

263 We identified 24,784 genes (transcripts with distinct gene symbols) in the transcriptome
264 (**Figure 1B, Table S1**). On the other hand, we identified 2,872 proteins in the proteome,
265 of which 1,884 were quantified in the 6 study samples (3WT and 3KO) (**Figure 1B, Figure**
266 **S2A, B, Table S2**). Of the proteins identified, 2,504 could be unambiguously associated
267 with a gene. These protein-coding genes (PCG) identified in the proteome covered 10%
268 of the total number of genes identified in the transcriptome (**Figure 1B**).

269 Our expression analysis (*ALMS1* KO vs WT) revealed a total of 1,712 differentially
270 expressed genes (DEG) and 158 differentially expressed proteins (DEG) (FDR < 0.05;
271 **Figure 1C, D**). Although the number of DEG detected in the proteome was 10 times
272 lower than in the transcriptome, a similar gene expression profile was observed in both
273 data sets (**Figure 1C, D**). Hence, despite the different resolution of these techniques,
274 they are consistent with each other (**Figure 1B**).

275

276 RNA-seq profiling of *ALMS1*-deficient BJ-5ta cells reveals
 277 different pathways related to extracellular matrix regulation:



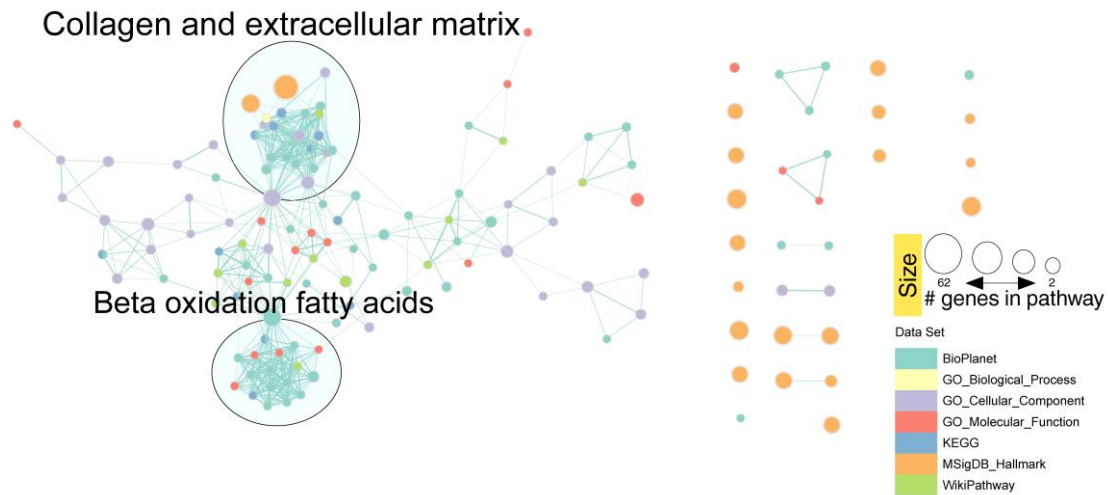
278

279 **Figure 2.** RNA-seq expression profile and enrichment analysis in the *ALMS1* knockout cell line
 280 (hTERT-BJ-5ta). **(A)** Heatmap of the 1,712 differentially expressed genes with FDR < 0.05 in the
 281 hTERT-BJ-5ta cell line after 24 hours with TGF- β pathway stimulation **(B)** The 20 most statistically
 282 significant GO terms detected after over-representation analysis (ORA) in the transcriptome. BP:
 283 biological process; CC: cellular Component **(C)** Signalling pathways significantly enriched (ORA,
 284 FDR < 0.01) for transcriptomic data in Bioplanet, KEGG, MSigDB and Wikipathway databases.

285 In the transcriptome, of 1,712 DEG, 1,119 (65%) were under-expressed and 593 (35%)
 286 were over-expressed in the *ALMS1* KO cell line compared to controls **(Figure 2A; Table**
 287 **S1).**

288 To determine the processes affected by inhibition of *ALMS1* gene expression in the
 289 transcriptome, we performed an over-representation analysis (ORA) **(Table S3)**. DEGs
 290 were not filtered by fold change (FC) due to the additive effect of small FCs along a
 291 signalling pathway **(Methods)**.

292 We found changes in the gene expression profile of *ALMS1* KO cell line in pathways
293 related to extracellular matrix (ECM) regulation through TGF- β , the Epithelial
294 Mesenchyme Transition (EMT) and various pathways that cross-signal with the TGF- β
295 pathway (BDNF, p53, TNF- α , EGFR1, KRAS and mTORC1) (**Figure 2B, C**).



296

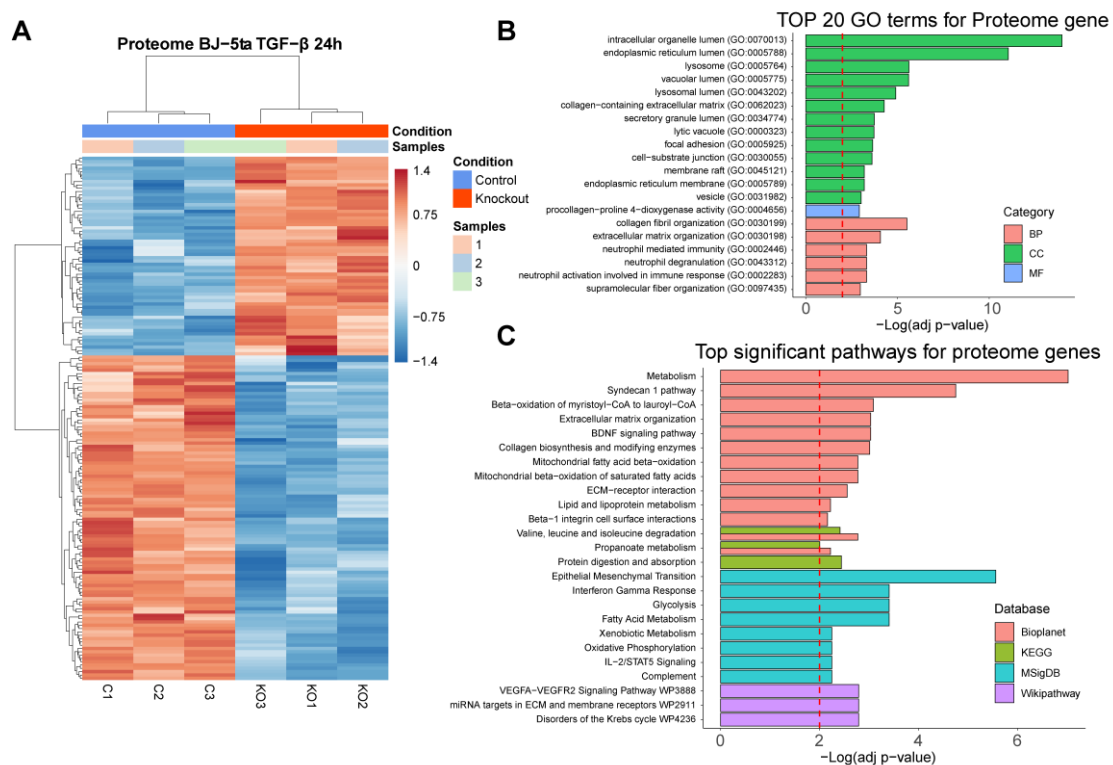
297 **Figure 3.** Network clustering of transcriptomic GO terms and enriched routes in the different
298 databases after applying the Markov clustering algorithm (MCL).

299 Next, we constructed a network using EnrichmentMap (Merico et al., 2010) to reduce
300 the redundancy of pathways and processes between the different databases used in the
301 previous analysis. For this, only enrichR terms with an FDR < 0.05 were used (**Methods**).
302 In this network, we found two main clusters, highly connected to each other,
303 incorporating pathways from different databases. The most representative keywords in
304 these clusters pointed towards collagen and ECM regulation and β -oxidation of fatty
305 acids (**Figure 3**).

306

307 **Proteomic profiling of *ALMS1*-deficient BJ-5ta cells suggests**
 308 **alterations in intracellular organelles lumen and lipid**
 309 **metabolism:**

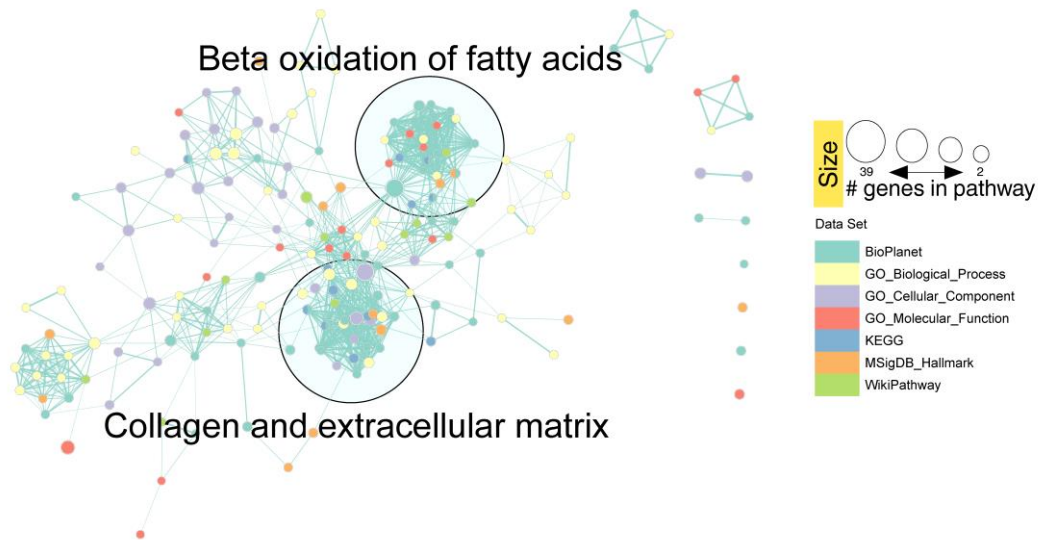
310 To study whether the observed differences in gene expression profile are replicated at
 311 the protein level, we performed the same analysis on the proteome (**Table S2**). Of 158
 312 DEG, 98 (62%) were under-expressed and 60 (38%) were over-expressed in the *ALMS1*
 313 KO cell line (**Figure 4A**).



314
 315 **Figure 4.** Protein expression profiling and enrichment analysis of *ALMS1* knockout cell line
 316 (hTERT-BJ-5ta). **(A)** Heatmap of the 158 differentially expressed protein coding genes with FDR
 317 < 0.05 in the hTERT-BJ-5ta cell line after 24 hours with TGF- β pathway stimulation **(B)** The 20
 318 most statistically significant GO terms detected after over-representation analysis (ORA) in the
 319 proteome. BP: biological process; CC: cellular Component; MF: molecular function **(C)** Signalling
 320 pathways significantly enriched (ORA, FDR < 0.01) for proteomic data in Bioplanet, KEGG,
 321 MSigDB and Wikipathway databases.

322 We performed an ORA to establish the proteome-enriched pathways and GOterms
 323 (**Table S4**). The proteome GO terms suggested that depletion of *ALMS1* gene affects the

324 endoplasmic reticulum, lysosomes, focal adhesion and the organisation of collagen and
325 ECM regulation (**Figure 4B**). These results are consistent with transcriptome findings,
326 including BDNF, Syndecan-1 signalling pathways and EMT (**Figure 4C**). In addition, other
327 enriched proteomic pathways involved in metabolic processes such as β -oxidation of
328 fatty acids in mitochondria were also detected (**Figure 4C**).



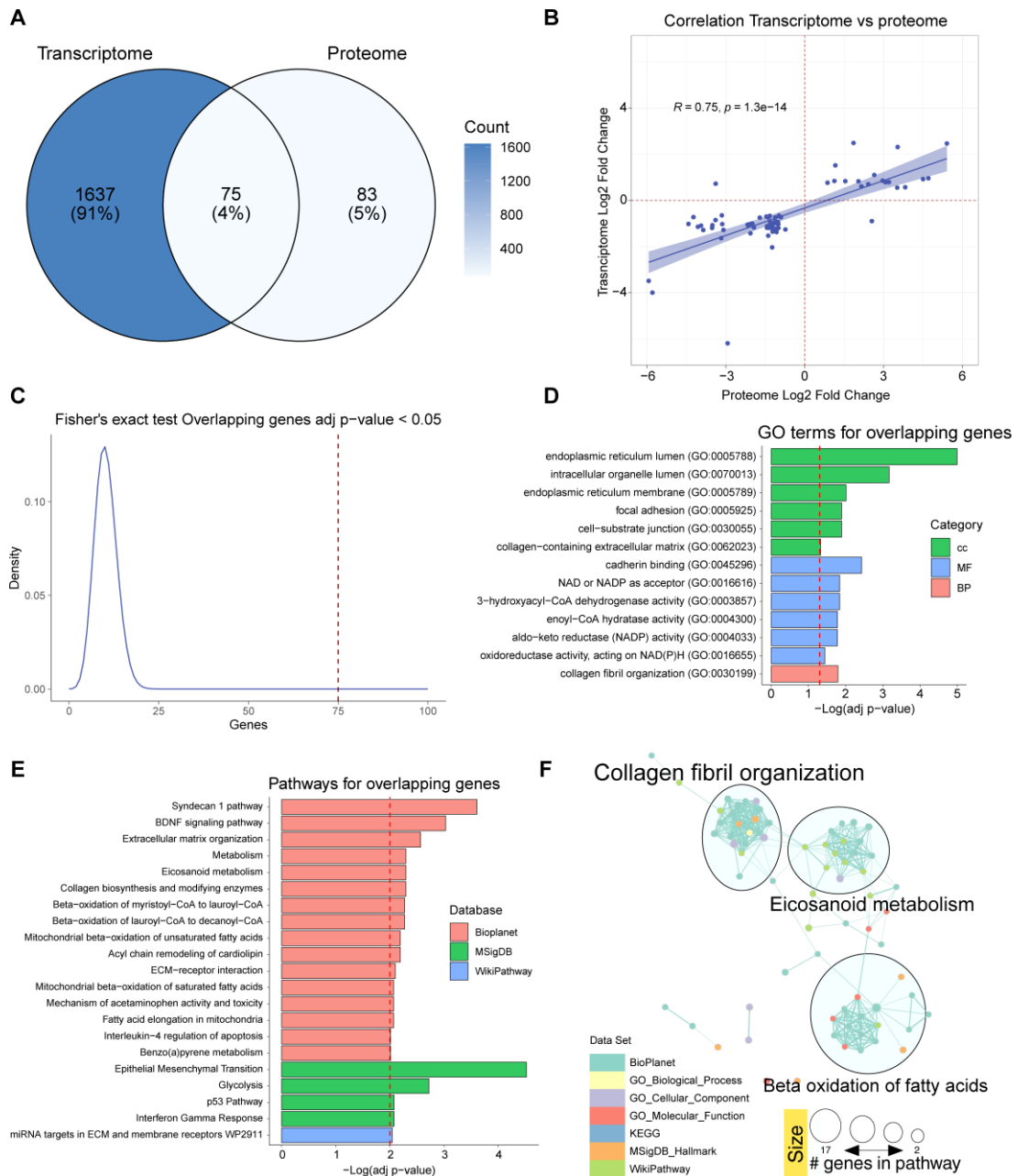
329

330 **Figure 5.** Network clustering of proteomic GO terms and enriched routes in the different
331 databases after applying the Markov clustering algorithm (MCL).

332 Regarding the reduction of redundancy between the databases used for the enrichment
333 analysis, we applied the same methodology as in the previous case, obtaining consistent
334 results with the transcriptome. We found two main clusters, associated with collagen
335 and ECM regulation and β -oxidation of fatty acids (**Figure 5**).

336

337 **The multi-omics analysis highlights the association of ALMS1**
 338 **with the endoplasmic reticulum, Syndecan-1 pathway and EMT:**



339

340 **Figure 6.** Analysis of differentially expressed genes overlapping between transcriptome and
 341 proteome. **(A)** Venn diagram with differentially expressed genes in the transcriptome and
 342 proteome and matching terms in both datasets. **(B)** Correlation plot between Log2 FCs in the
 343 transcriptome and the proteome of the matched terms. **(C)** Fisher's exact test to evaluate the
 344 probability of obtaining 75 or more matched genes. **(D)** Significantly over-represented (ORA, FDR
 345 < 0.05) GO terms that are associated with the subset of matched data. **(E)** Significantly over-

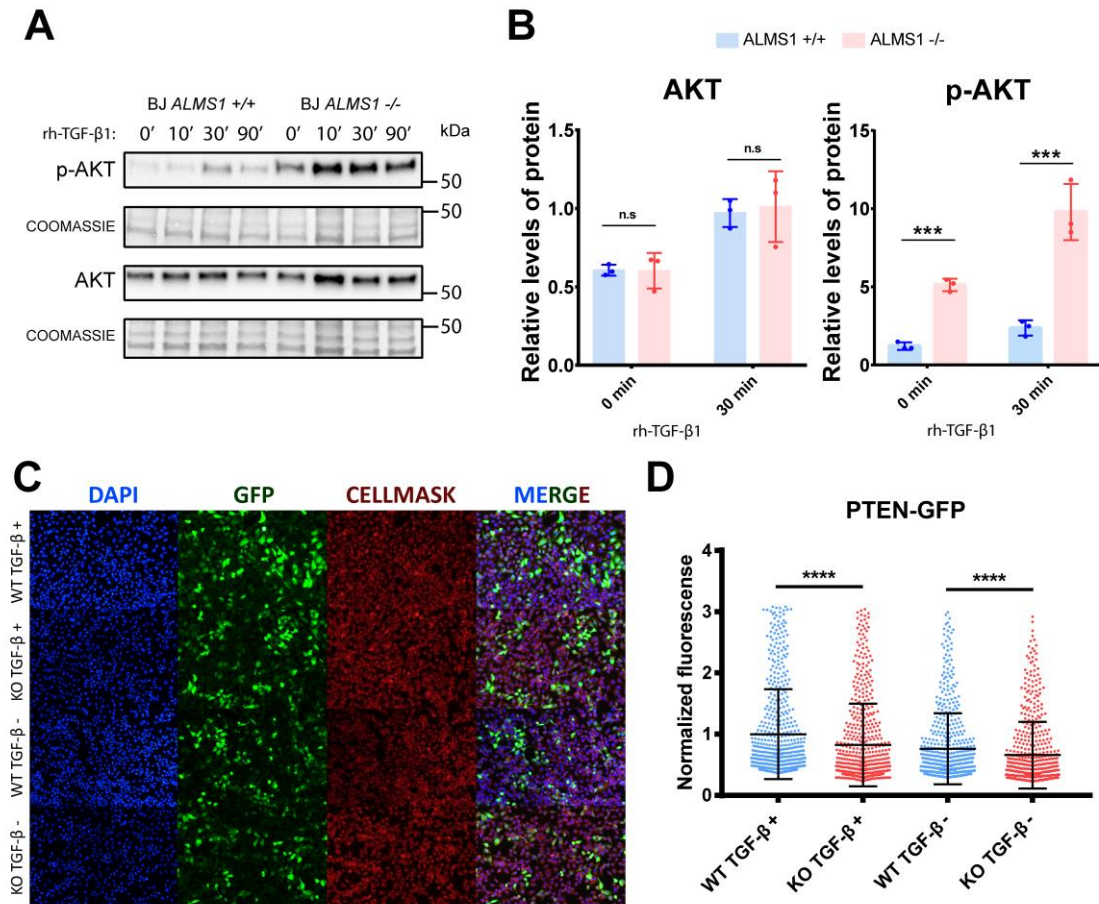
346 represented pathways (ORA, FDR < 0.01) in the list of overlapping genes **(F)**. Network clustering
347 of GO terms and pathways in the different bases of the overlapping gene data after applying the
348 Markov clustering algorithm (MCL).

349 To investigate the relationship between the transcriptome and proteome, we analysed
350 the overlap of DEG between them (1,712 genes and 158 proteins). This resulted in 75
351 DEG in the *ALMS1* KO cell line **(Figure 6A; Table S5)** with a Pearson correlation of 0.75
352 (p-value 1.3×10^{-14}) between the FCs of the transcriptome and proteome **(Figure 6B)**.
353 Importantly, the likelihood of finding by chance 75 or more common DEG between the
354 transcriptome and proteome is practically zero (Fisher's exact test). Thus, these genes
355 are a valid signature of *ALMS1* depletion **(Figure 6C)**.

356 Further, their enrichment analysis highlights the role of *ALMS1* in the endoplasmic
357 reticulum, BDNF or Syndecan 1 pathways, EMT and lipid-associated signalling pathways
358 such as fatty acid metabolism **(Figure 6D, E; Table S6)**. This time, the enriched pathway
359 reduction analysis identified three clusters, one cluster agglutinated the alterations of
360 the ECM, another the alterations of the β -oxidation of fatty acids and the third cluster
361 highlighted the metabolism of eicosanoids, which also affects lipid metabolism **(Figure**
362 **6F)**.

363 ***ALMS1* depletion affects the signalling cross-talk between TGF- β** 364 **and PI3K/AKT:**

365 *ALMS1* depletion does not appear to affect the activation of the canonical TGF- β
366 pathway in all cell types (Bea-Mascato et al., 2022) so the observed alterations could be
367 due to aberrant signalling of non-canonical pathways such as PI3K/AKT. The PI3K/AKT
368 pathway regulates many of the altered processes found in our analyses. This pathway is
369 involved in control of cell migration, proliferation and adhesion (Xu et al., 2015; Yu and
370 Cui, 2016) as well as in cell metabolism (Yu and Cui, 2016; Hoxhaj and Manning, 2019).
371 Given the present results, we decided to study the cross-signalling between the TGF- β
372 and PI3K/AKT pathway in our *ALMS1*-deficient fibroblast line.



373

374 **Figure 7.** Study of cross-signalling between TGF-β and AKT pathways in ALMS1KO cell models.
 375 **(A)** Representative Western blot of AKT overactivation after TGF-β pathway stimulation in BJ-
 376 5ta. **(B)** Quantification of AKT protein expression and p-AKT activation levels normalised against
 377 Coomassie staining in BJ-5ta. **(C)** Representative images of fluorescence labelling of HeLa cells
 378 after transfection with GFP-tagged PTEN. **(D)** Normalised fluorescence of the 550 most
 379 fluorescent HeLa cells in each preparation.

380 For this purpose, AKT protein phosphorylation levels were measured in the hTERT-BJ-
 381 5ta *ALMS1* KO cell line by Western blot at four different stimulation times with TGF-β1
 382 ligand (0, 10, 30 and 90 min). Indeed, deficiency of *ALMS1* generates an over-activation
 383 of the AKT pathway (**Figure 7A, B**). This over-activation was present at basal level (time
 384 0), but was exacerbated by TGF-β stimulation, with the differentials between ALMS1KO
 385 and WT being most notable in AKT after 30min of TGF-β1 stimulation (**Figure 7A, B**).

386 We thus hypothesised that over-activation of the AKT pathway results from the
 387 accumulation of membrane phospholipids such as PIP3, which is the substrate for the

388 activation of PI3K and subsequently AKT. The PTEN protein is responsible for
389 dephosphorylating PIP3 to PIP2 which inhibits the AKT pathway. For this reason, the
390 PTEN inhibition could be a cause of the AKT over-activation. To test this hypothesis, we
391 transfected a KO model for the *ALMS1* gene in the HeLa cell line with a plasmid to
392 express PTEN protein fused to GFP. We observed a significant reduction of GFP
393 fluorescence in the KO cells compared with controls in both untreated and TGF- β ligand-
394 treated cells (p-value < 0.0001). This suggests that *ALMS1* depletion affects PTEN
395 expression. Moreover, this inhibition seems to be slightly accentuated (p-value < 0.01)
396 after TGF- β stimulation (**Figure 7C, D**).

397

398 **DISCUSSION:**

399 While the role of the centrosome in the control of the mitotic cycle has been very well
400 studied, little is known about its structure and functions in other contexts (Doxsey et al.,
401 2005; Bettencourt-Dias and Glover, 2007; Conduit et al., 2015). The study of different
402 mutated centrosomal proteins and their impact on processes of the primary cilium, such
403 as ciliogenesis, endocytosis or the signalling of various pathways such as WNT, SHh or
404 TGF- β , has however been enlightening (Kobayashi and Dynlacht, 2011; Collin et al.,
405 2012; Hehnlly et al., 2012; Leitch et al., 2014; Mönnich et al., 2018; Gonçalves et al.,
406 2021). Despite all this, many of the regulatory aspects of how centrosomal proteins
407 coordinate these processes remain unknown.

408 The TGF- β signalling is one of the main pathways regulated through the primary cilium
409 (Clement et al., 2013). It is involved in normal development in mammals and influences
410 other pathways by cross-signalling such as p53, MAPKs or PI3K/AKT (Rahimi and Leof,
411 2007; Patel et al., 2019; Finnson et al., 2020). For this reason, it is timely to determine
412 the role of different ciliary and basal body genes, such as *ALMS1*, in their regulation.

413 Thus, we further explored the previously described association between *ALMS1*
414 deficiency and alterations in TGF- β -mediated signal transduction (Álvarez-Satta et al.,
415 2021; Bea-Mascato et al., 2022). We performed gene expression profiling by RNA-seq
416 and LFQ-proteomics in an *ALMS1*KO hTERT-BJ-5ta cell line stimulated with TGF- β 1. This
417 cellular model was previously generated and characterised in our lab (Bea-Mascato et
418 al., 2022). We found that the lack of *ALMS1* generates an inhibited gene expression
419 profile after TGF- β 1 stimulation, both in the transcriptome and proteome (**Figure 2A;**
420 **4A**). This gene expression profile is consistent with our previously described proteomic
421 results in HeLa and with the basal gene expression profile described in patient
422 fibroblasts (Zulato et al., 2011; Bea-Mascato et al., 2022). This means that the lack of
423 *ALMS1* is likely to have an inhibitory impact on most of the processes controlled
424 downstream of this gene, such as mitosis, cell migration or receptor recycling. (Zulato et
425 al., 2011; Leitch et al., 2014; Shenje et al., 2014; Bea-Mascato et al., 2022).

426 The ORA of transcriptome revealed alterations in the TGF- β signalling pathway and other
427 tangentially regulated pathways such as mTOR, EGFR or p53 and processes such as ECM

428 regulation or EMT (**Figure 2B, C**). The existence of this cross-signalling is known,
429 however, this is the first time that the impact of ALMS1 depletion on it has been shown,
430 which could open up new avenues of treatment for ALMS patients. (Kato et al., 2009;
431 Hamidi et al., 2017; Patel et al., 2019). On the other hand, It was previously established,
432 that ALMS1 depletion led to aberrant expression of several TGF- β 1-induced EMT
433 markers in HeLa and hTERT-BJ-5ta cells (Bea-Mascato et al., 2022). However, these
434 results further establish the connection between ALMS1 depletion and EMT alterations.
435 EMT inhibition supports the poor migration capacity of cells lacking ALMS1 which may
436 be due to cytoskeleton collapse, another event described in cells lacking ALMS1 (Zulato
437 et al., 2011; Collin et al., 2012; Bea-Mascato et al., 2022).

438 Downstream activation of the TGF- β pathway can follow *via* the canonical pathway,
439 dependent on SMADs (SMAD2 and SMAD3), or non-canonical, which encompasses a
440 plethora of pathways such as MAPKs, ERKs, p53, or PI3K/AKT (Finnson et al., 2020). For
441 this reason, alterations in cross-signalling pathways such as mTORC1, EGFR1 or p53
442 detected in the transcriptome show that alterations in TGF- β are mainly related to the
443 non-canonical part of this pathway (**Figure 2C**) (Patel et al., 2019; Finnson et al., 2020).

444 Our proteomic analysis revealed proteins involved in lipid metabolism and cytoplasmic
445 organelles such as the endoplasmic reticulum, mitochondria, or lysosomes (**Figure 4B,**
446 **C**). We have previously described that ALMS1 depletion does impact cell viability due to
447 changes in mitochondrial reduction capacity (Bea-Mascato et al., 2022). However, it
448 appears to affect mitochondrial β -oxidation of fatty acids (**Figure 4C**). This could connect
449 the absence of ALMS1 to oxidative metabolism disorders (Liu and Desai, 2015). In
450 addition, alterations in cytoplasmic organelles, such as the endoplasmic reticulum and
451 lysosomes, could be related to alterations in endocytosis, receptor recycling or
452 autophagy. ALMS1 absence has been linked to alterations in transferrin (TfR), NOTCH
453 and NKCC2 receptor recycling, but its role in TGF- β receptor recycling or autophagy has
454 not yet been established (Collin et al., 2012; Leitch et al., 2014; Jaykumar et al., 2018;
455 Yang et al., 2020).

456 Indeed, after applying a redundancy reduction analysis of enriched pathways, we found
457 that ALMS1 regulates two main clusters in the transcriptome and proteome; processes
458 related to the regulation of the ECM and processes related to lipid metabolism such as

459 β -oxidation of fatty acids (**Figure 3; 5**). It has already been described that deletion of
460 *ALMS1* leads to overexpression of several ECM components in fibroblasts from ALMS
461 patients. For this reason, understanding these alterations is key to determining the
462 pathophysiology of fibrosis in ALMS (Zulato et al., 2011). On the other hand, the
463 metabolic alterations observed in ALMS could have their origin in processes such as β -
464 oxidation of fatty acids (Romano et al., 2008; Huang-Doran and Semple, 2010; Favaretto
465 et al., 2014; Geberhiwot et al., 2021).

466 The list of common differentially expressed genes between the transcriptome and
467 proteome supports the above findings, indicating that *ALMS1* depletion affects EMT,
468 endoplasmic reticulum, Syndecan-1 and BDNF signalling pathways and lipid metabolism
469 pathways such as β -oxidation of fatty acids (**Figure 6D, E**) (Kasza et al., 2014). By studying
470 this list of genes by redundancy reduction analysis, we saw the existence of a link
471 between *ALMS1* depletion and eicosanoid metabolism in addition to the processes
472 mentioned above (**Figure 6F**). Alterations related to the ECM are undoubtedly key to the
473 appearance of fibrosis in these patients; however, alterations in the β -oxidation of fatty
474 acids, beyond their link to obesity, may contribute to the appearance of fibrotic tissue
475 due to lipid deposits (Serra et al., 2013; Kang et al., 2014). This suggest that the
476 metabolic disorder in patients with ALMS is involved in the progressive development of
477 fibrosis in various organs such as the kidneys and liver (Bettini et al., 2021).

478 Regarding the deregulation of the PI3K/AKT, we can relate the over-activation of AKT
479 (**Figure 7A, B**) with the inhibition of the p53 pathway (**Figure 1C**) (Gottlieb et al., 2002;
480 Abraham and O'Neill, 2014). This is supported by the decrease in the expression of the
481 *PTEN* gene, which could explain an over-phosphorylation of the cell membrane and an
482 accumulation of PIP3 leading to the over-activation of AKT (**Figure 7C, D**) (Álvarez-Garcia
483 et al., 2019). To our knowledge, this is the first study to explore how *ALMS1* affects cross-
484 signalling between AKT and the TGF- β pathway. Other studies have been carried out to
485 try to understand the role of *ALMS1* in regulating the insulin mediated AKT pathway.
486 The involvement of AKT has not yet been clearly established in ALMS, while some studies
487 in pre-adipocytes have not detected any differences in AKT activation, other studies in
488 mice have shown that AKT is over-activated in some tissues and it is inhibited in others,
489 when *ALMS1* is depleted (Huang-Doran and Semple, 2010; Favaretto et al., 2014;

490 Geberhiwot et al., 2021). AKT regulation is tissue specific, it has 3 distinct isoforms and
491 each has multiple phosphorylation sites (Liao and Hung, 2010). This could be an
492 explanation for the disparity of the data present in the bibliography.

493 The over-activation of the AKT pathway could be the link between alterations at the
494 metabolic level and alterations related to the ECM. The inhibition of p53 would be
495 caused by this over-activation through MDM2, affecting the PTEN-p53-AKT-MDM2 loop
496 (Gottlieb et al., 2002; Abraham and O'Neill, 2014). This hypothesis would be supported
497 by the resistance to apoptosis in *ALMS1*-depleted cells (Zulato et al., 2011; Bea-Mascato
498 et al., 2022).

499 **CONCLUSION:**

500 In conclusion, the lack of *ALMS1* gene expression alters the TGF- β pathway in the
501 knockout cell model. It also seems to compromise the signalling of other tangential
502 pathways such as PI3K/AKT or p53. These signalling alterations appear to affect diverse
503 metabolic processes involving the mitochondrial, endoplasmic reticulum and lysosomes
504 and various lipid-mediated signalling pathways. The alterations are mainly clustered into
505 processes affecting the regulation of the ECM and the β -oxidation of fatty acids, which
506 we confirmed in both the transcriptome and proteome. Finally, *ALMS1* depletion led to
507 over-activation of the AKT protein in BJ-5ta cells and inhibition of the PTEN protein in
508 HeLa cells.

509 **Author Contributions:** BB-M, DV designed the study. BB-M performed the experiments.
510 EG-C, YS-C and SC assisted with RNA-seq analysis and data integration. All authors wrote
511 the manuscript and provided approval for publication.

512 **Funding:** This work was funded by Instituto de Salud Carlos III de Madrid FIS project
513 PI15/00049 and PI19/00332, Xunta de Galicia (Centro de Investigación de Galicia CINBIO
514 2019-2022) Ref. ED431G-2019/06, Consolidación e estruturación de unidades de
515 investigación competitivas e outras accións de fomento (ED431C-2018/54). Brais Bea-
516 Mascato (FPU17/01567) was supported by graduate studentship awards (FPU
517 predoctoral fellowship) from the Spanish Ministry of Education, Culture and Sports. We
518 thank the NIHR GOSH BRC for its support (to YE S-C and SC).

519 **Informed Consent Statement:** Not Apply.

520 **Data Availability Statement:** Data are available via Gene Expression Omnibus (GEO)
521 with the identifier GSE209844 and ProteomeXchange with the identifier PXD035708.

522 **Code Availability Statement:** The code used in this study can be accessed at the GitHub
523 address "https://github.com/BreisOne/multiomic_pipeline".

524 **Acknowledgements:** We sincerely thank the Proteomics and Genomics services from
525 Centro de Apoyo Científico-Tecnológico a la Investigación (CACTI) of University of Vigo
526 and its specialists Paula Álvarez Chaver, Ángel Sebastián Comesaña, Verónica Outeiriño
527 and Manuel Marcos for their guidance and advise. We also thank Mercedes Peleteiro
528 Olmedo from Centro de Investigaci3n Biomédicas (CINBIO) from University of Vigo for
529 the flow cytometry service.

530 **Conflicts of Interest:** The authors declare no conflict of interest. The funders had no role
531 in the design of the study; in the collection, analyses, or interpretation of data; in the
532 writing of the manuscript, or in the decision to publish the results.

533

534 REFERENCES:

- 535 Abraham, A. G., and O'Neill, E. (2014). PI3K/Akt-mediated regulation of p53 in cancer.
536 *Biochem. Soc. Trans.* 42, 798–803. doi: 10.1042/BST20140070.
- 537 Álvarez-García, V., Tawil, Y., Wise, H. M., and Leslie, N. R. (2019). Mechanisms of PTEN
538 loss in cancer: It's all about diversity. *Semin. Cancer Biol.* 59, 66–79. doi:
539 10.1016/J.SEMCANCER.2019.02.001.
- 540 Álvarez-Satta, M., Lago-Docampo, M., Bea-Mascato, B., Solarat, C., Castro-Sánchez, S.,
541 Christensen, S. T., et al. (2021). ALMS1 Regulates TGF- β Signaling and Morphology
542 of Primary Cilia. *Front. Cell Dev. Biol.* 9, 112. Available at:
543 <https://www.frontiersin.org/article/10.3389/fcell.2021.623829>.
- 544 Anders, S., Pyl, P. T., and Huber, W. (2015). HTSeq—a Python framework to work with
545 high-throughput sequencing data. *Bioinformatics* 31, 166–169. doi:
546 10.1093/bioinformatics/btu638.
- 547 Anvarian, Z., Mykytyn, K., Mukhopadhyay, S., Pedersen, L. B., and Christensen, S. T.
548 (2019). Cellular signalling by primary cilia in development, organ function and
549 disease. *Nat. Rev. Nephrol.* 15, 199–219. doi: 10.1038/s41581-019-0116-9.
- 550 Barrett, T., Wilhite, S. E., Ledoux, P., Evangelista, C., Kim, I. F., Tomashevsky, M., et al.
551 (2013). NCBI GEO: archive for functional genomics data sets—update. *Nucleic Acids*
552 *Res.* 41, D991. doi: 10.1093/NAR/GKS1193.
- 553 Bea-Mascato, B., Neira-Goyanes, E., Iglesias-Rodríguez, A., and Valverde, D. (2022).
554 Depletion of ALMS1 affects TGF- β signalling pathway and downstream processes
555 such as cell migration and adhesion capacity. *Front. Mol. Biosci.* 0, 1085. doi:
556 10.1101/2021.12.19.473196.
- 557 Bettencourt-Dias, M., and Glover, D. M. (2007). Centrosome biogenesis and function:
558 centrosomics brings new understanding. *Nat. Rev. Mol. Cell Biol.* 8, 451–463. doi:
559 10.1038/NRM2180.
- 560 Bettini, S., Bombonato, G., Dassie, F., Favaretto, F., Piffer, L., Bizzotto, P., et al. (2021).
561 Liver Fibrosis and Steatosis in Alström Syndrome: A Genetic Model for Metabolic

- 562 Syndrome. *Diagnostics* 2021, Vol. 11, Page 797 11, 797. doi:
563 10.3390/DIAGNOSTICS11050797.
- 564 Chen, J.-H., Geberhiwot, T., Barrett, T. G., Paisey, R., and Semple, R. K. (2017). Refining
565 genotype-phenotype correlation in Alström syndrome through study of primary
566 human fibroblasts. *Mol. Genet. genomic Med.* 5, 390–404. doi: 10.1002/mgg3.296.
- 567 Christensen, S. T., Morthorst, S. K., Mogensen, J. B., and Pedersen, L. B. (2017). Primary
568 Cilia and Coordination of Receptor Tyrosine Kinase (RTK) and Transforming Growth
569 Factor β (TGF- β) Signaling. *Cold Spring Harb. Perspect. Biol.* 9, a028167. doi:
570 10.1101/CSHPERSPECT.A028167.
- 571 Clement, C. A., Ajbrou, K. D., Koefoed, K., Vestergaard, M. L., Veland, I. R., Henriques de
572 Jesus, M. P. R., et al. (2013). TGF- β signaling is associated with endocytosis at the
573 pocket region of the primary cilium. *Cell Rep.* 3, 1806–14. doi:
574 10.1016/j.celrep.2013.05.020.
- 575 Collin, G. B., Cyr, E., Bronson, R., Marshall, J. D., Gifford, E. J., Hicks, W., et al. (2005).
576 *Alms1*-disrupted mice recapitulate human Alström syndrome. *Hum. Mol. Genet.*
577 14, 2323–2333. doi: 10.1093/hmg/ddi235.
- 578 Collin, G. B., Marshall, J. D., Ikeda, A., So, W. V., Russell-Eggitt, I., Maffei, P., et al. (2002).
579 Mutations in *ALMS1* cause obesity, type 2 diabetes and neurosensory degeneration
580 in Alström syndrome. *Nat. Genet.* 31, 74–8. doi: 10.1038/ng867.
- 581 Collin, G. B., Marshall, J. D., King, B. L., Milan, G., Maffei, P., Jagger, D. J., et al. (2012).
582 The Alström syndrome protein, *ALMS1*, interacts with α -actinin and components of
583 the endosome recycling pathway. *PLoS One* 7, e37925–e37925. doi:
584 10.1371/journal.pone.0037925.
- 585 Conduit, P. T., Wainman, A., and Raff, J. W. (2015). Centrosome function and assembly
586 in animal cells. *Nat. Rev. Mol. Cell Biol.* 16, 611–624. doi: 10.1038/NRM4062.
- 587 Dobin, A., Davis, C. A., Schlesinger, F., Drenkow, J., Zaleski, C., Jha, S., et al. (2013). STAR:
588 ultrafast universal RNA-seq aligner. *Bioinformatics* 29, 15–21. doi:
589 10.1093/bioinformatics/bts635.

- 590 Doxsey, S., Zimmerman, W., and Mikule, K. (2005). Centrosome control of the cell cycle.
591 *Trends Cell Biol.* 15, 303–311. doi: 10.1016/J.TCB.2005.04.008.
- 592 Ewels, P., Magnusson, M., Lundin, S., and Källér, M. (2016). MultiQC: summarize analysis
593 results for multiple tools and samples in a single report. *Bioinformatics* 32, 3047–
594 3048. doi: 10.1093/BIOINFORMATICS/BTW354.
- 595 Favaretto, F., Milan, G., Collin, G. B., Marshall, J. D., Stasi, F., Maffei, P., et al. (2014).
596 GLUT4 Defects in Adipose Tissue Are Early Signs of Metabolic Alterations in
597 Alms1GT/GT, a Mouse Model for Obesity and Insulin Resistance. *PLoS One* 9,
598 e109540. doi: 10.1371/JOURNAL.PONE.0109540.
- 599 Finnson, K. W., Almadani, Y., and Philip, A. (2020). Non-canonical (non-SMAD2/3) TGF- β
600 signaling in fibrosis: Mechanisms and targets. *Semin. Cell Dev. Biol.* 101, 115–122.
601 doi: 10.1016/J.SEMCDB.2019.11.013.
- 602 Geberhiwot, T., Baig, S., Obringer, C., Girard, D., Dawson, C., Manolopoulos, K., et al.
603 (2021). Relative Adipose Tissue Failure in Alström Syndrome Drives Obesity-
604 Induced Insulin Resistance. *Diabetes* 70, 364–376. doi: 10.2337/DB20-0647.
- 605 Gonçalves, A. B., Hasselbalch, S. K., Joensen, B. B., Patzke, S., Martens, P., Ohlsen, S. K.,
606 et al. (2021). CEP78 functions downstream of CEP350 to control biogenesis of
607 primary cilia by negatively regulating CP110 levels. *Elife* 10. doi:
608 10.7554/ELIFE.63731.
- 609 Gottlieb, T. M., Martinez Leal, J. F., Seger, R., Taya, Y., and Oren, M. (2002). Cross-talk
610 between Akt, p53 and Mdm2: possible implications for the regulation of apoptosis.
611 *Oncogene* 2002 218 21, 1299–1303. doi: 10.1038/sj.onc.1205181.
- 612 Graser, S., Stierhof, Y.-D., Lavoie, S. B., Gassner, O. S., Lamla, S., Le Clech, M., et al.
613 (2007). Cep164, a novel centriole appendage protein required for primary cilium
614 formation. *J. Cell Biol.* 179, 321–330. doi: 10.1083/jcb.200707181.
- 615 Hamidi, A., Song, J., Thakur, N., Itoh, S., Marcusson, A., Bergh, A., et al. (2017). TGF- β
616 promotes PI3K-AKT signaling and prostate cancer cell migration through the TRAF6-
617 mediated ubiquitylation of p85 α . *Sci. Signal.* 10. doi: 10.1126/SCISIGNAL.AAL4186.

- 618 Hearn, T. (2018). ALMS1 and Alström syndrome: a recessive form of metabolic,
619 neurosensory and cardiac deficits. *J. Mol. Med.* doi: 10.1007/s00109-018-1714-x.
- 620 Hearn, T., Spalluto, C., Phillips, V. J., Renforth, G. L., Copin, N., Hanley, N. A., et al. (2005).
621 Subcellular Localization of ALMS1 Supports Involvement of Centrosome and Basal
622 Body Dysfunction in the Pathogenesis of Obesity, Insulin Resistance, and Type 2
623 Diabetes. *Diabetes* 54, 1581 LP – 1587. doi: 10.2337/diabetes.54.5.1581.
- 624 Hehnly, H., Chen, C. T., Powers, C. M., Liu, H. L., and Doxsey, S. (2012). The Centrosome
625 Regulates the Rab11- Dependent Recycling Endosome Pathway at Appendages of
626 the Mother Centriole. *Curr. Biol.* 22, 1944–1950. doi: 10.1016/J.CUB.2012.08.022.
- 627 Hoxhaj, G., and Manning, B. D. (2019). The PI3K–AKT network at the interface of
628 oncogenic signalling and cancer metabolism. *Nat. Rev. Cancer* 2019 202 20, 74–88.
629 doi: 10.1038/s41568-019-0216-7.
- 630 Huang-Doran, I., and Semple, R. K. (2010). Knockdown of the Alström syndrome-
631 associated gene *Alms1* in 3T3-L1 preadipocytes impairs adipogenesis but has no
632 effect on cell-autonomous insulin action. *Int. J. Obes.* 2010 3410 34, 1554–1558.
633 doi: 10.1038/ijo.2010.92.
- 634 Ishikawa, H., and Marshall, W. F. (2011). Ciliogenesis: building the cell’s antenna. *Nat.*
635 *Rev. Mol. Cell Biol.* 12, 222–234. doi: 10.1038/NRM3085.
- 636 Jagger, D., Collin, G., Kelly, J., Towers, E., Nevill, G., Longo-Guess, C., et al. (2011). Alström
637 Syndrome protein ALMS1 localizes to basal bodies of cochlear hair cells and
638 regulates cilium-dependent planar cell polarity. *Hum. Mol. Genet.* 20, 466–481. doi:
639 10.1093/hmg/ddq493.
- 640 Jaykumar, A. B., Caceres, P. S., King-Medina, K. N., Liao, T.-D., Datta, I., Maskey, D., et al.
641 (2018). Role of Alström syndrome 1 in the regulation of blood pressure and renal
642 function. *JCI insight* 3, e95076. doi: 10.1172/jci.insight.95076.
- 643 Kang, H. M., Ahn, S. H., Choi, P., Ko, Y. A., Han, S. H., Chinga, F., et al. (2014). Defective
644 fatty acid oxidation in renal tubular epithelial cells has a key role in kidney fibrosis
645 development. *Nat. Med.* 2014 211 21, 37–46. doi: 10.1038/nm.3762.

- 646 Kasza, I., Suh, Y., Wollny, D., Clark, R. J., Roopra, A., Colman, R. J., et al. (2014). Syndecan-
647 1 Is Required to Maintain Intradermal Fat and Prevent Cold Stress. *PLOS Genet.* 10,
648 e1004514. doi: 10.1371/JOURNAL.PGEN.1004514.
- 649 Kato, M., Putta, S., Wang, M., Yuan, H., Lanting, L., Nair, I., et al. (2009). TGF-beta
650 activates Akt kinase through a microRNA-dependent amplifying circuit targeting
651 PTEN. *Nat. Cell Biol.* 11, 881–889. doi: 10.1038/NCB1897.
- 652 Knorz, V. J., Spalluto, C., Lessard, M., Purvis, T. L., Adigun, F. F., Collin, G. B., et al. (2010).
653 Centriolar association of ALMS1 and likely centrosomal functions of the ALMS
654 motif-containing proteins C10orf90 and KIAA1731. *Mol. Biol. Cell* 21, 3617–29. doi:
655 10.1091/mbc.E10-03-0246.
- 656 Kobayashi, T., and Dynlacht, B. D. (2011). Regulating the transition from centriole to
657 basal body. *J. Cell Biol.* 193, 435–444. doi: 10.1083/JCB.201101005.
- 658 Kuleshov, M. V., Jones, M. R., Rouillard, A. D., Fernandez, N. F., Duan, Q., Wang, Z., et al.
659 (2016). Enrichr: a comprehensive gene set enrichment analysis web server 2016
660 update. *Nucleic Acids Res.* 44, W90. doi: 10.1093/NAR/GKW377.
- 661 Leitch, C. C., Lodh, S., Prieto-Echagüe, V., Badano, J. L., and Zaghloul, N. A. (2014). Basal
662 body proteins regulate Notch signaling through endosomal trafficking. *J. Cell Sci.*
663 127, 2407–19. doi: 10.1242/jcs.130344.
- 664 Li, G., Vega, R., Nelms, K., Gekakis, N., Goodnow, C., McNamara, P., et al. (2007). A role
665 for Alström syndrome protein, *alms1*, in kidney ciliogenesis and cellular quiescence.
666 *PLoS Genet.* 3, e8. doi: 10.1371/journal.pgen.0030008.
- 667 Liao, Y., and Hung, M. C. (2010). Physiological regulation of Akt activity and stability. *Am.*
668 *J. Transl. Res.* 2, 19. Available at: /pmc/articles/PMC2826820/ [Accessed August 22,
669 2022].
- 670 Liu, R. M., and Desai, L. P. (2015). Reciprocal regulation of TGF- β and reactive oxygen
671 species: A perverse cycle for fibrosis. *Redox Biol.* 6, 565. doi:
672 10.1016/J.REDOX.2015.09.009.
- 673 Love, M. I., Huber, W., and Anders, S. (2014). Moderated estimation of fold change and

- 674 dispersion for RNA-seq data with DESeq2. *Genome Biol.* 15, 550. doi:
675 10.1186/s13059-014-0550-8.
- 676 May-Simera, H. L., Wan, Q., Jha, B. S., Hartford, J., Khristov, V., Dejene, R., et al. (2018).
677 Primary Cilium-Mediated Retinal Pigment Epithelium Maturation Is Disrupted in
678 Ciliopathy Patient Cells. *Cell Rep.* 22, 189–205. doi: 10.1016/j.celrep.2017.12.038.
- 679 May-Simera, H., Nagel-Wolfrum, K., and Wolfrum, U. (2017). Cilia - The sensory
680 antennae in the eye. *Prog. Retin. Eye Res.* 60, 144–180. doi:
681 10.1016/J.PRETEYERES.2017.05.001.
- 682 Merico, D., Isserlin, R., Stueker, O., Emili, A., and Bader, G. D. (2010). Enrichment Map:
683 A Network-Based Method for Gene-Set Enrichment Visualization and
684 Interpretation. *PLoS One* 5, e13984. doi: 10.1371/JOURNAL.PONE.0013984.
- 685 Mönnich, M., Borgeskov, L., Breslin, L., Jakobsen, L., Rogowski, M., Doganli, C., et al.
686 (2018). CEP128 Localizes to the Subdistal Appendages of the Mother Centriole and
687 Regulates TGF- β /BMP Signaling at the Primary Cilium. *Cell Rep.* 22, 2584–2592. doi:
688 10.1016/J.CELREP.2018.02.043.
- 689 Pala, R., Alomari, N., and Nauli, S. M. (2017). Primary Cilium-Dependent Signaling
690 Mechanisms. *Int. J. Mol. Sci.* 18. doi: 10.3390/IJMS18112272.
- 691 Patel, S., Tang, J., Overstreet, J. M., Anorga, S., Lian, F., Arnouk, A., et al. (2019). Rac-
692 GTPase promotes fibrotic TGF- β 1 signaling and chronic kidney disease via EGFR,
693 p53, and Hippo/YAP/TAZ pathways. *FASEB J.* 33, 9797–9810. doi:
694 10.1096/FJ.201802489RR.
- 695 Perez-Riverol, Y., Csordas, A., Bai, J., Bernal-Llinares, M., Hewapathirana, S., Kundu, D.
696 J., et al. (2019). The PRIDE database and related tools and resources in 2019:
697 improving support for quantification data. *Nucleic Acids Res.* 47, D442–D450. doi:
698 10.1093/nar/gky1106.
- 699 Rahimi, R. A., and Leof, E. B. (2007). TGF- β signaling: A tale of two responses. *J. Cell.*
700 *Biochem.* 102, 593–608. doi: 10.1002/JCB.21501.
- 701 Reimand, J., Isserlin, R., Voisin, V., Kucera, M., Tannus-Lopes, C., Rostamianfar, A., et al.

- 702 (2019). Pathway enrichment analysis and visualization of omics data using
703 g:Profiler, GSEA, Cytoscape and EnrichmentMap. *Nat. Protoc.* 14, 482–517. doi:
704 10.1038/S41596-018-0103-9.
- 705 Ritchie, M. E., Phipson, B., Wu, D., Hu, Y., Law, C. W., Shi, W., et al. (2015). limma powers
706 differential expression analyses for RNA-sequencing and microarray studies.
707 *Nucleic Acids Res.* 43, e47–e47. doi: 10.1093/NAR/GKV007.
- 708 Romano, S., Milan, G., Veronese, C., Collin, G. B., Marshall, J. D., Centobene, C., et al.
709 (2008). Regulation of Alström syndrome gene expression during adipogenesis and
710 its relationship with fat cell insulin sensitivity. *Int. J. Mol. Med.* 21, 731–736. doi:
711 10.3892/IJMM.21.6.731/HTML.
- 712 Schindelin, J., Arganda-Carreras, I., Frise, E., Kaynig, V., Longair, M., Pietzsch, T., et al.
713 (2012). Fiji: an open-source platform for biological-image analysis. *Nat. Methods*
714 *2012* 9, 676–682. doi: 10.1038/nmeth.2019.
- 715 Serra, D., Mera, P., Malandrino, M. I., Mir, J. F., and Herrero, L. (2013). Mitochondrial
716 Fatty Acid Oxidation in Obesity. <https://home.liebertpub.com/ars> 19, 269–284. doi:
717 10.1089/ARS.2012.4875.
- 718 Shenje, L. T., Andersen, P., Halushka, M. K., Lui, C., Fernandez, L., Collin, G. B., et al.
719 (2014). Mutations in Alström protein impair terminal differentiation of
720 cardiomyocytes. *Nat. Commun.* 5, 3416. doi: 10.1038/ncomms4416.
- 721 Varet, H., Brillet-Guéguen, L., Coppée, J.-Y., and Dillies, M.-A. (2016). SARTools: A
722 DESeq2- and EdgeR-Based R Pipeline for Comprehensive Differential Analysis of
723 RNA-Seq Data. *PLoS One* 11, e0157022. Available at:
724 <https://doi.org/10.1371/journal.pone.0157022>.
- 725 Wickham, H. (2016). *ggplot2: Elegant Graphics for Data Analysis*. Springer-Verlag New
726 York Available at: <https://ggplot2.tidyverse.org>.
- 727 Xu, W., Yang, Z., and Lu, N. (2015). A new role for the PI3K/Akt signaling pathway in the
728 epithelial-mesenchymal transition.
729 <http://dx.doi.org/10.1080/19336918.2015.1016686> 9, 317–324. doi:
730 10.1080/19336918.2015.1016686.

- 731 Yang, C., Chen, X. C., Li, Z. H., Wu, H. L., Jing, K. P., Huang, X. R., et al. (2020). SMAD3
732 promotes autophagy dysregulation by triggering lysosome depletion in tubular
733 epithelial cells in diabetic nephropathy. *https://doi.org/10.1080/15548627.2020.1824694* 17, 2325–2344. doi:
734 [10.1080/15548627.2020.1824694](https://doi.org/10.1080/15548627.2020.1824694).
735
- 736 Yu, J. S. L., and Cui, W. (2016). Proliferation, survival and metabolism: the role of
737 PI3K/AKT/mTOR signalling in pluripotency and cell fate determination.
738 *Development* 143, 3050–3060. doi: [10.1242/DEV.137075](https://doi.org/10.1242/DEV.137075).
- 739 Zhang, X., Smits, A. H., van Tilburg, G. B., Ovaa, H., Huber, W., and Vermeulen, M. (2018).
740 Proteome-wide identification of ubiquitin interactions using UbiA-MS. *Nat. Protoc.*
741 13, 530–550. doi: [10.1038/nprot.2017.147](https://doi.org/10.1038/nprot.2017.147).
- 742 Zulato, E., Favaretto, F., Veronese, C., Campanaro, S., Marshall, J. D., Romano, S., et al.
743 (2011). ALMS1-deficient fibroblasts over-express extra-cellular matrix components,
744 display cell cycle delay and are resistant to apoptosis. *PLoS One* 6, e19081–e19081.
745 doi: [10.1371/journal.pone.0019081](https://doi.org/10.1371/journal.pone.0019081).
746